



THE UNIVERSITY *of* EDINBURGH

Edinburgh Research Explorer

Integrative analysis of multi-platform reverse-phase protein array data for the pharmacodynamic assessment of response to targeted therapies

Citation for published version:

Byron, A, Bernhardt, S, Ouine, B, Cartier, A, Macleod, K, Carragher, N, Sibut, V, Korf, U, Serrels, B & de Koning, L 2020, 'Integrative analysis of multi-platform reverse-phase protein array data for the pharmacodynamic assessment of response to targeted therapies', *Scientific Reports*.
<https://doi.org/10.1038/s41598-020-77335-0>

Digital Object Identifier (DOI):

[10.1038/s41598-020-77335-0](https://doi.org/10.1038/s41598-020-77335-0)

Link:

[Link to publication record in Edinburgh Research Explorer](#)

Document Version:

Publisher's PDF, also known as Version of record

Published In:

Scientific Reports

General rights

Copyright for the publications made accessible via the Edinburgh Research Explorer is retained by the author(s) and / or other copyright owners and it is a condition of accessing these publications that users recognise and abide by the legal requirements associated with these rights.

Take down policy






The University of Edinburgh has made every reasonable effort to ensure that Edinburgh Research Explorer content complies with UK legislation. If you believe that the public display of this file breaches copyright please contact openaccess@ed.ac.uk providing details, and we will remove access to the work immediately and investigate your claim.





OPEN

Integrative analysis of multi-platform reverse-phase protein array data for the pharmacodynamic assessment of response to targeted therapies

Adam Byron¹ , Stephan Bernhardt^{2,5} , Bérèngere Ouine³, Aurélie Cartier^{3,6}, Kenneth G. Macleod¹, Neil O. Carragher¹ , Vonick Sibut^{4,7}, Ulrike Korf², Bryan Serrels^{1,8}  & Leanne de Koning³ 

Reverse-phase protein array (RPPA) technology uses panels of high-specificity antibodies to measure proteins and protein post-translational modifications in cells and tissues. The approach offers sensitive and precise quantification of large numbers of samples and has thus found applications in the analysis of clinical and pre-clinical samples. For effective integration into drug development and clinical practice, robust assays with consistent results are essential. Leveraging a collaborative RPPA model, we set out to assess the variability between three different RPPA platforms using distinct instrument set-ups and workflows. Employing multiple RPPA-based approaches operated across distinct laboratories, we characterised a range of human breast cancer cells and their protein-level responses to two clinically relevant cancer drugs. We integrated multi-platform RPPA data and used unsupervised learning to identify protein expression and phosphorylation signatures that were not dependent on RPPA platform and analysis workflow. Our findings indicate that proteomic analyses of cancer cell lines using different RPPA platforms can identify concordant profiles of response to pharmacological inhibition, including when using different antibodies to measure the same target antigens. These results highlight the robustness and the reproducibility of RPPA technology and its capacity to identify protein markers of disease or response to therapy.

In the era of personalised medicine and targeted cancer therapies, identifying those patients that will benefit from existing and new therapies is paramount. Genetics is already being used to assist clinical decision-making in specific cases¹, but additional levels of biological information are required to better understand disease and more accurately predict phenotype from genotype². A crucial source of information in this context is the proteome and, notably, the activation status of dynamic cell signalling pathways through post-translational protein modifications. Indeed, genomic mutations are not always associated with activated signalling pathways and, conversely, pathway activation can occur in the absence of mutations, as exemplified by *PIK3CA*³ and human epidermal growth factor receptor 2 (Her2, also known as ErbB2) signalling⁴ in breast cancer.

¹Cancer Research UK Edinburgh Centre, Institute of Genetics and Molecular Medicine, University of Edinburgh, Crewe Road South, Edinburgh EH4 2XR, UK. ²Division of Molecular Genome Analysis, German Cancer Research Center (DKFZ), Heidelberg, Germany. ³Department of Translational Research, Institut Curie, PSL Research University, 26 rue d'Ulm, 75005 Paris, France. ⁴U900 INSERM, Institut Curie, PSL Research University, Paris, France. ⁵Present address: Pfizer Pharma GmbH, Berlin, Germany. ⁶Present address: Sederma, Le Perray-en-Yvelines, France. ⁷Present address: U1236 INSERM, Faculté de Médecine, Université de Rennes 1, Rennes, France. ⁸Present address: NanoString Technologies, Inc., Seattle, WA, USA. ✉email: adam.byron@igmm.ed.ac.uk; leanne.de-koning@curie.fr

Several technologies exist for protein biomarker discovery and validation^{5–7}, among which reverse-phase protein array (RPPA) is a technology of choice for its unequalled sample throughput. The RPPA technology uses panels of monospecific affinity reagents (usually validated, high-quality antibodies) to quantify, with high precision and sensitivity, the abundance of specific proteins and their post-translationally modified forms in biological specimens^{8,9}. Protein samples derived from cells or tissues are immobilised on a solid substrate, deposited as small spots on multiple arrays, and each array is probed with a single, epitope-specific antibody. This enables simultaneous quantification of multiple proteins and post-translational modifications in hundreds of samples, a multiplex capability not available in any other current proteomic technology. The capacity to analyse large sample numbers enables analysis of multiple sample conditions, such as drug treatments, dose responses and time courses, resulting in data series that can support systems biology and drug discovery pipelines^{10,11}. The high sensitivity (in the picomole–femtomole range) and good reproducibility of RPPA technology^{8,12–16} have motivated its application to a wide range of sample types, including cell lines, preclinical (e.g. xenograft) models and patient-derived material. Indeed, the microscale printing of very small amounts of samples is of particular benefit for analysis of limited clinical or preclinical material, and RPPA has become a powerful addition to the biomedical analytical toolbox for the investigation of disease mechanisms, diagnostics and prognostics, notably in cancer^{17–26}.

The RPPA workflow is composed of several distinct steps, which can each be adapted to the needs of the laboratory or the study. RPPAs thus offer a highly flexible, modular proteomic technology, enabling numerous possible technical set-ups and protocols. As most laboratories using RPPA technology have developed a customised set-up, there are essentially as many workflows as there are RPPA platforms. Differences between platforms are diverse and can include the type of printer used to create the arrays, sample spotting conditions, slide substrate chemistry, primary and secondary antibodies used for immunostaining and slide scanner optics²⁷. Moreover, no standard tools exist to quantify, normalise and quality control RPPA data. Several RPPA data processing methods have been developed^{16,28–40}, but these are often designed for specific technical set-ups, requiring, for example, particular array layouts or raw data formats. To our knowledge, no extensive cross-platform validation has been reported for RPPA technology. There is, therefore, a need to assess and understand the impact of variation between RPPA data derived from different platforms across international research centres.

As RPPA workflows are being developed for use in clinical settings, for which robust assays are paramount^{41,42}, there is a growing need for the evaluation of the reproducibility of RPPA platform outputs. Herein, we use collaborative RPPA-based proteomics, employing distinct RPPA workflows at multiple research sites in different countries, to characterise a range of human breast cancer cell lines and their biochemical responses to two clinically relevant cancer drugs. We combine data derived from different RPPA platforms to assess inter-platform variation and use integrative analysis to identify platform-independent protein markers of response to drug treatment. Such cross-platform validation may thus have utility in multi-centre evaluation of robust protein markers of disease and therapeutic response.

Results

Multi-platform RPPA analysis of breast cancer cell lines. To assess the reproducibility of RPPA technology across multiple laboratories, we developed an international multi-platform approach that integrated RPPA data derived from three research sites across Europe (Paris, France; Heidelberg, Germany; Edinburgh, United Kingdom). We selected for this study six breast cancer cell lines, encompassing different breast cancer molecular subtypes and presenting distinct drug sensitivities (Supplementary Table S1). The cells were cultured in the absence or presence of two kinase inhibitors for 20 min or 24 h and lysed in biological triplicate. In total, we generated 108 snap-frozen lysates, which were shipped to the three research sites (Fig. 1a). Samples were analysed at each site using the respective in-house RPPA platforms, the set-up of which differed at many stages of the RPPA analysis workflow, including slide type, the number of technical replicates and dilutions per sample, read-out dye, scanner, image analysis software and normalisation procedure (Supplementary Table S2), enabling the capture of variation between RPPA platforms operated in different laboratories. Microarrayed samples were probed with panels of validated antibodies in routine use on the three RPPA platforms. To enable dataset comparison, all antibodies were assigned unique antibody identifiers, and only data derived from antibodies targeting the same protein(s) or phosphorylated residue(s) (including different antibodies from different suppliers) acquired on all three RPPA platforms were used for further analysis (Supplementary Table S3). This experimental design thus enabled the assessment of inter-platform concordance.

First, RPPA data of the six breast cancer cell lines cultured under control conditions were analysed using the respective in-house data analysis procedures of the three research sites. Analysis of these control samples generated in biological triplicate with antibodies used in the multi-platform RPPA analysis resulted in 522, 558 and 486 antibody readings (processed signal intensities) for the Paris, Heidelberg and Edinburgh platforms, respectively. Normalised RPPA data derived from each platform were then clustered antibody-wise to identify similarities between validated antibodies (Supplementary Table S4). For each RPPA platform, clusters containing antibodies targeting the same protein or phosphoprotein were identified, indicating that normalised intensity profiles across cell types correlated for subsets of different antibodies (Fig. 1b–d, Supplementary Fig. S1). Most distinct antibodies targeting the same antigen, such as phosphorylated Erk1/2, clustered together in each RPPA dataset, indicating consistent results for the same antigen (Fig. 1e–g, Supplementary Fig. S1). In addition, antibodies targeting different phosphorylated residues on the same protein or antibodies targeting phosphorylated and corresponding total proteins, such as for S6 ribosomal protein or mTOR, generally clustered together in each RPPA dataset, although the degree of correlation varied between RPPA platforms and distance metrics (Fig. 1b–d, Supplementary Fig. S1). These data suggest that many of the antibodies routinely used for RPPA analysis at the three research sites in this study give comparable results relative to the rest of each dataset.

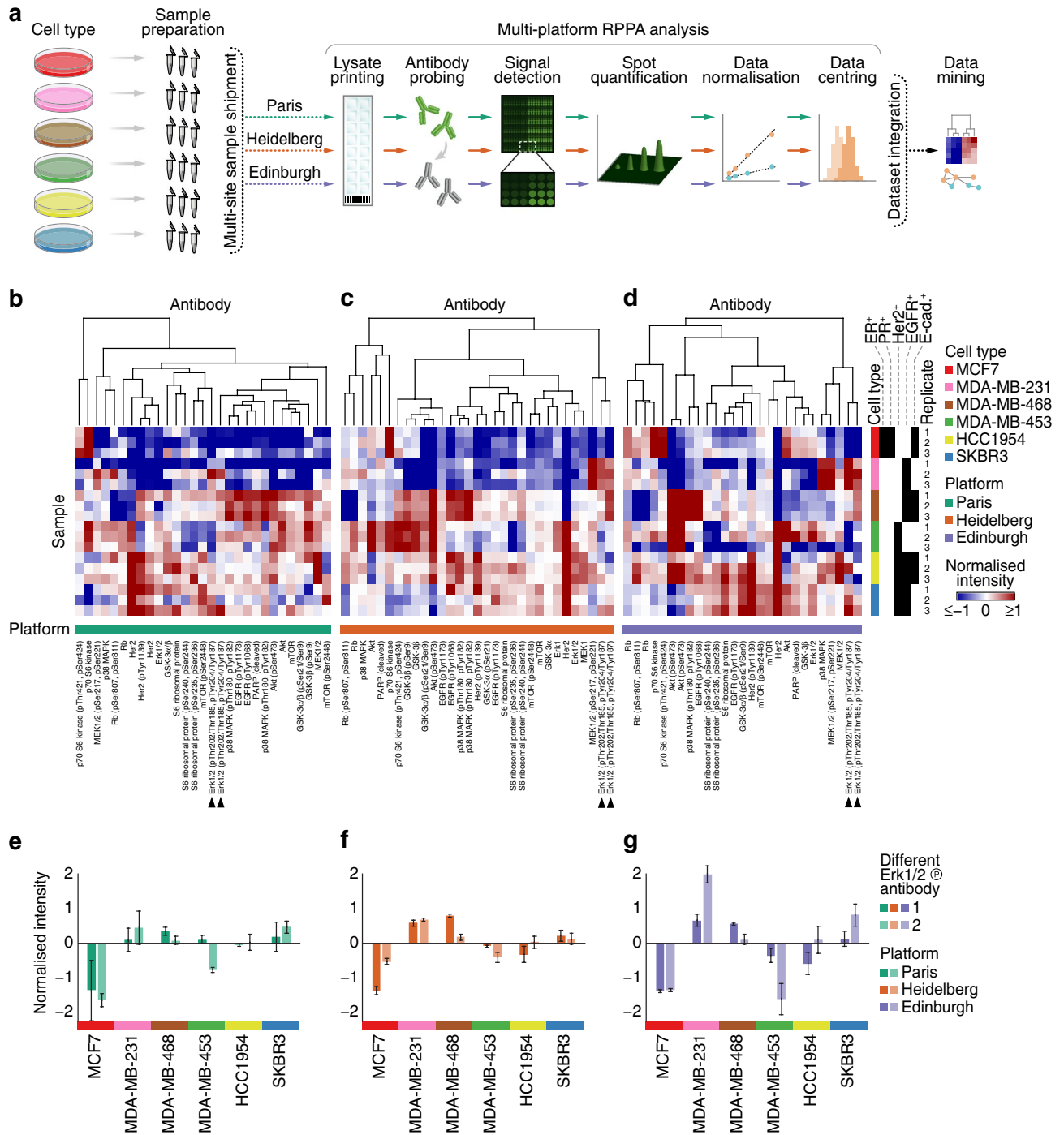


Figure 1. Multi-platform RPPA analysis of breast cancer cell lines. **(a)** Schematic illustration of the multi-platform RPPA workflow. Images created using Illustrator. **(b–d)** Hierarchical cluster analysis of RPPA data of six breast cancer cell lines cultured under control conditions derived from three RPPA platforms. RPPA data derived from the Paris **(b)**, Heidelberg **(c)** and Edinburgh **(d)** platforms were clustered on the basis of antibody-wise dissimilarity (Spearman rank correlation coefficient-based distance). Clustering was performed separately for each platform, and sample order was maintained for each cluster analysis. Annotation bars indicate cell type, cell type receptor status and RPPA platform. Arrowheads indicate different phosphorylated Erk1/2 antibodies. **(e–g)** RPPA data for phosphorylated Erk1/2 (pThr202/Thr185, pTyr204/Tyr187) derived from the Paris **(e)**, Heidelberg **(f)** and Edinburgh **(g)** RPPA platforms. All three platforms used the same two antibodies that recognise phosphorylated Erk1/2 (dark bars, antibody identifier Erk1/2_pThr202/Thr185,pTyr204/Tyr187_a; light bars, antibody identifier Erk1/2_pThr202/Thr185,pTyr204/Tyr187_b). Annotation bars (x-axis) indicate cell type. Data are means \pm s.e.m. ($n = 3$ independent samples). For further details, see Supplementary Fig. S1 and Supplementary Table S4.

Integrative analysis of multi-platform RPPA data. To assess the comparability of RPPA data originating from multiple platforms, we integrated normalised RPPA data for control samples derived from each platform (1566 antibody readings) and analysed the integrated dataset using unsupervised learning. For dataset integration, antigens targeted by each antibody were classified, capturing antibody recognition of related protein isoforms or family members where applicable (e.g. antibodies recognising Erk1 and Erk1/2 were linked and assigned the same antibody antigen class, Erk1/2). Each data point was linked to the RPPA platform from which it was derived to enable downstream data analysis. We reduced the dimensionality of the integrated multi-platform RPPA dataset using principal component analysis. This unsupervised analysis of the six breast cancer cell lines revealed separation in feature space for several of the cell types, indicating cell type-specific expression of the proteins and phosphoproteins measured (Fig. 2a). Next, two-dimensional hierarchical cluster analysis of the integrated dataset, using multiple distinct distance functions to quantify dissimilarity between data points in the feature space, partitioned samples by breast cancer cell line, elucidating discriminatory profiles of protein and phosphoprotein expression for each cell type (Fig. 2b, Supplementary Fig. S2). Moreover, unsupervised cluster analysis identified correlated subsets of antibodies targeting the same antigens. The data driving these antibody clusters were generally derived from multiple RPPA platforms and, where available, using different antibodies (Fig. 2b, Supplementary Table S5), suggesting that the profiles of protein and phosphoprotein expression were comparable between RPPA platform set-ups.

To interrogate the similarity between antigen expression profiles for distinct antibodies used on different RPPA platforms, we devised a data-driven representation of antibody similarity, which we termed a clustered antibody antigen map. Antibodies used at each RPPA platform (clustered as for Fig. 2b) were annotated with their respective antigens (classified as described in “Methods”). With clustered antibodies as columns, antigen annotations were expanded into rows of a matrix. The resulting matrix was populated with unique antibody identifiers to distinguish different antibodies, from which a heatmap of clustered antibody–antigen space was generated. Thus, the antibody antigen map provides detailed annotation of cluster analysis of multi-platform RPPA data. This enables identification of clustered antibodies that recognise antigens with similar expression profiles across the integrated dataset (Fig. 2b,c, Supplementary Fig. S2).

The antibody antigen map revealed that the expression of many of the antigens tested (71%) clustered with expression of the same antigen determined by at least one other RPPA platform (Fig. 2c,d). In addition, the expression of several of the antigens for which distinct antibodies were used (61%) clustered with the same antigen detected by a different antibody (Fig. 2c,d). Together, these results indicate that RPPA analyses performed at different research sites using distinct set-ups can identify concordant sets of distinct antibodies that target the same antigens. This implies that different high-quality, validated antibodies can be used to generate consistent results from the same samples using different RPPA platforms.

Consistency of multi-platform RPPA analysis of drug-treated breast cancer cell lines. To analyse the robustness of RPPA technology using a more relevant ‘intervention’ dataset (i.e. including treatment conditions), we extended the integrative analysis to include multi-platform RPPA data of the six breast cancer cell lines treated with two clinically relevant drugs, lapatinib (Tykerb, Tyverb) and selumetinib (AZD6244, ARRY-142886). Lapatinib is a reversible ATP-mimetic tyrosine kinase inhibitor of epidermal growth factor receptor (EGFR, also known as ErbB1) and Her2⁴³; selumetinib is a selective ATP-independent allosteric inhibitor of mitogen-activated protein kinase kinase (MAPKK, also known as MEK)⁴⁴. To capture the signalling dynamics of the proteins under investigation, cells were treated with either drug or with DMSO (vehicle control) for 20 min and 24 h (Fig. 3a).

First, to examine the consistency of results generated by the antibodies used in the multi-platform RPPA analysis, we calculated correlations between all-sample RPPA data derived from all antibodies tested, which consisted of 9,396 antibody readings. This analysis showed that RPPA data derived from antibodies recognising the same antigen class (i.e. ‘like’ antigens) were generally well correlated (median Spearman rank correlation coefficient, $r_s = 0.70$) (Fig. 3b). In contrast, data derived from all antibodies—regardless of target—were generally poorly correlated ($r_s = 0.22$), as expected (Fig. 3b), implying that RPPA-based quantification of like target antigens is in substantially better agreement than quantification of random antigens in the dataset. Notably, RPPA data for antigens recognised by the same antibody were correlated to a similar level to those recognised by different antibodies (Fig. 3c), indicating that distinct, validated antibodies generate consistent results from the same samples. In addition, correlations between normalised RPPA data derived from all antibodies were lower than those between corresponding raw RPPA data, resulting in a better separation of correlation distributions for like antigens and for all antibodies (Supplementary Fig. S3). This suggests that normalisation of RPPA data better differentiates concordant data (derived from antibodies recognising the same antigen class) from less-concordant data (derived from all antibodies regardless of target).

To assess the reproducibility of RPPA results across different RPPA platforms, we compared correlation distributions for like antigens for each pair-wise combination of platforms. Each platform comparison showed a similar correlation distribution for antigens recognised by the same antibodies (Fig. 3d) and a similar correlation distribution for antigens recognised by different antibodies (Fig. 3e), although different antibodies used at the Paris and Edinburgh platforms were less well correlated. Strong positive correlations between platforms did not appear to be restricted to high-intensity RPPA data (Supplementary Fig. S3), suggesting that the observed correlation distributions were not driven solely by samples with high levels of antigen expression. Importantly, antigens detected by different antibodies used at different RPPA platforms were, in general, almost as well correlated as those used at the same RPPA platform (Fig. 3f). These data show that RPPA analyses of the same samples at different platforms using distinct workflows yield consistent results, including when several different antibodies are used to recognise the same antigen (protein or phosphoprotein) of interest.

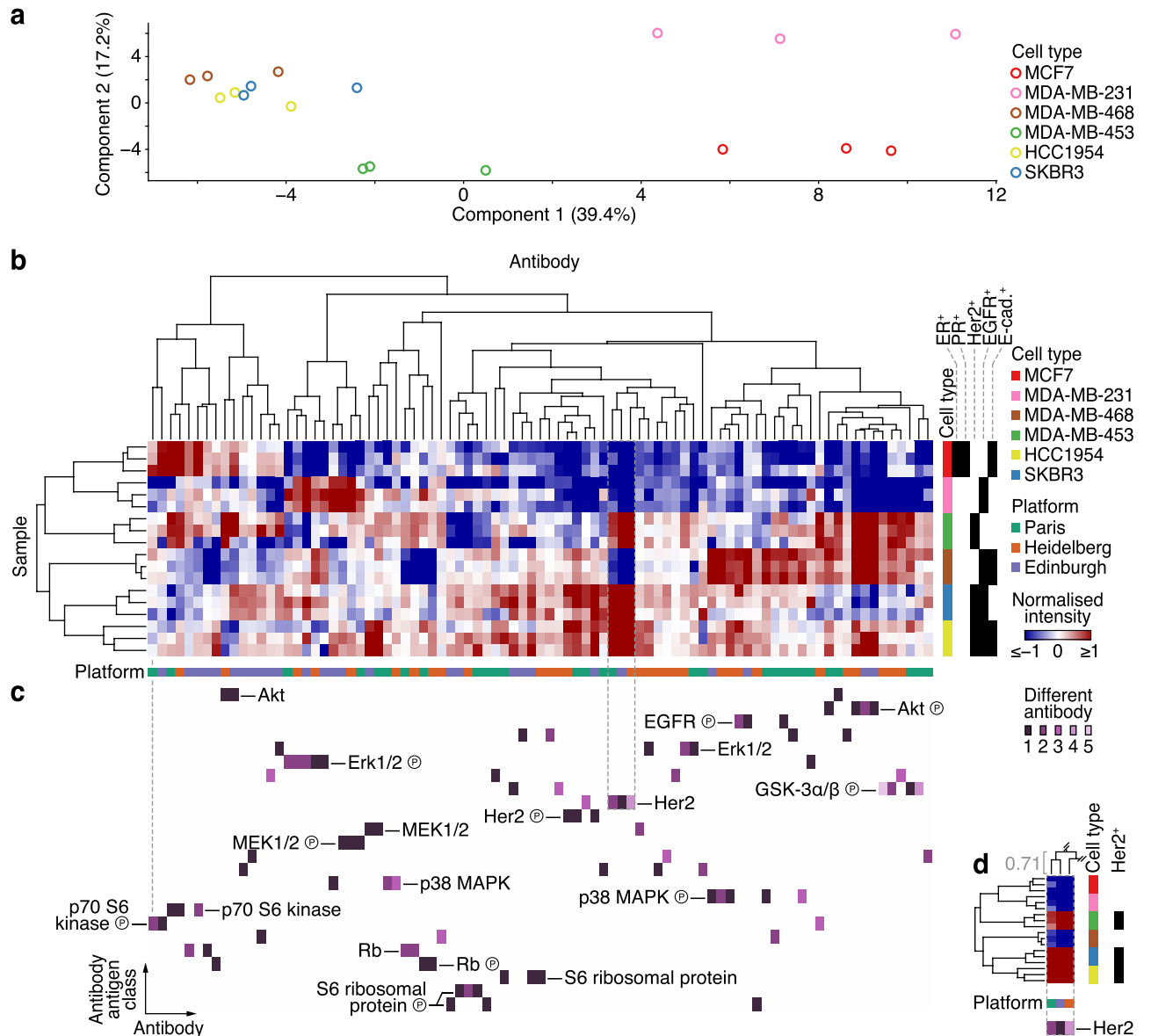


Figure 2. Integrative analysis of multi-platform RPPA data. **(a)** Principal component analysis of integrated multi-platform RPPA data of six breast cancer cell lines cultured under control conditions. **(b)** Integrated multi-platform RPPA data were clustered on the basis of antibody-wise and sample-wise dissimilarities (Spearman rank correlation coefficient-based distance). Annotation bars indicate cell type, cell type receptor status and RPPA platform. **(c)** Clustered antibody antigen map for all antibodies used in the integrative analysis. The map is aligned with the hierarchical clustering results in **(b)** [grey dashed line above the left-most antibody indicates alignment of the first antibody (column) end-node]. Distinct antibodies that target the same antigen class (unique antibody identifiers) are indicated by different shades of purple. Antibody antigen classes are ordered alphabetically for clarity. **(d)** Exemplar of clustered antibodies that recognise Her2, indicated by grey dashed box in **(b)** and **(c)**. Antibodies used by all three RPPA platforms clustered in antibody-antigen space. Spearman rank correlation coefficient of the cluster column node is shown in grey. All three platforms used different antibodies that recognise Her2 (antibody identifiers for Paris, Her2_b; Heidelberg, Her2_d; Edinburgh, Her2_a). For further details, see Supplementary Fig. S2 and Supplementary Table S5.

Integrative multi-platform RPPA analysis of drug-treated breast cancer cell lines. We hypothesised that the observed consistency of multi-platform RPPA data would allow robust detection of potential markers of cellular response to signalling pathway inhibition. To confirm overall changes in RPPA data upon drug treatment of breast cancer cells, we reduced the dimensionality of the integrated dataset using principal component analysis. Unsupervised analysis of all cell lines identified shifts in feature space away from control conditions for some drug-treated cells, suggesting cell type-specific differential regulation of proteins and phosphoproteins (Supplementary Fig. S4). For example, the Her2-amplified SKBR3 cell line is highly sensitive to lapatinib^{45,46}, and treatment with lapatinib induced substantial changes in phosphoprotein abundance, including

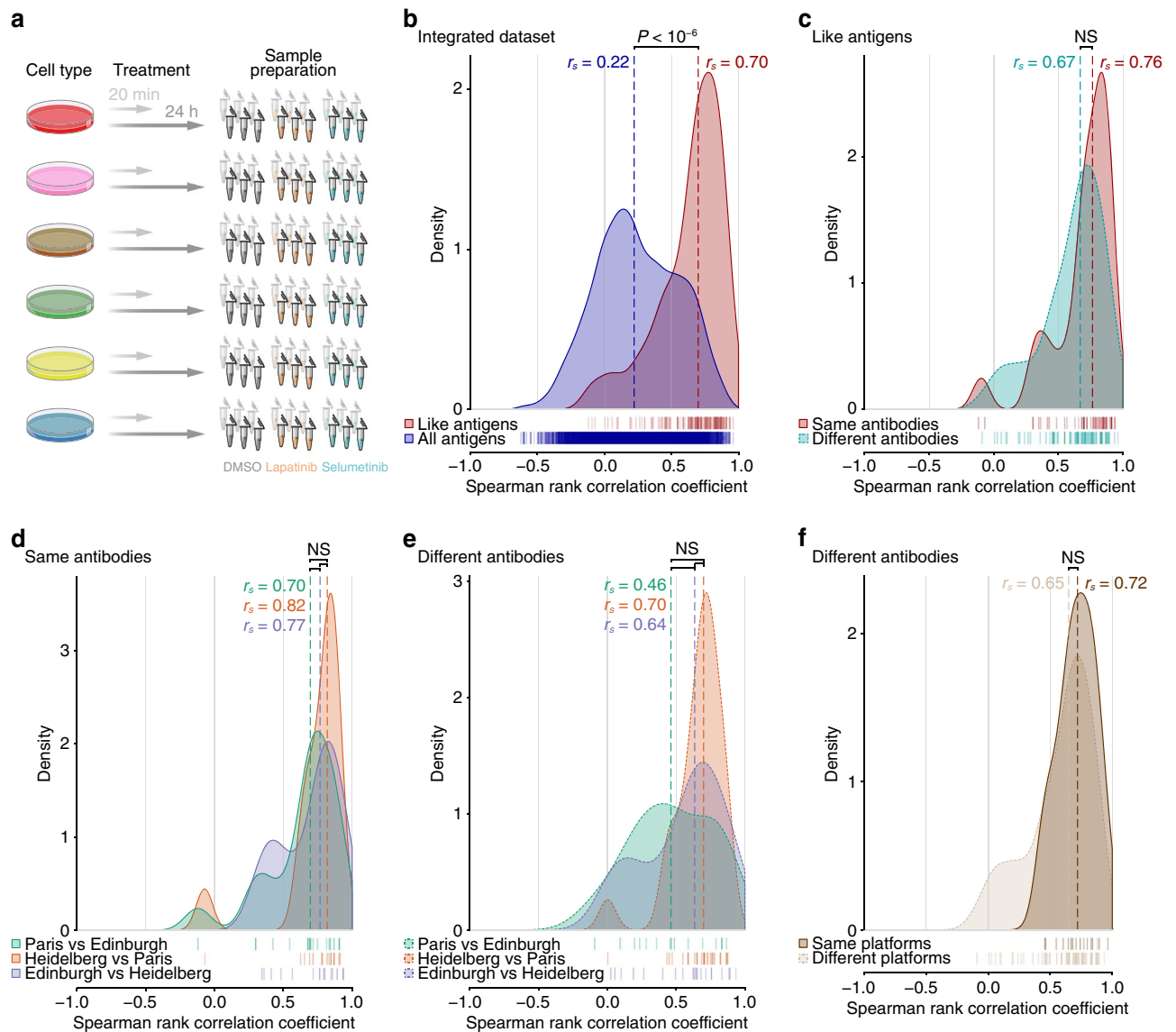


Figure 3. Correlations of RPPA data used for integrative analysis of drug-treated breast cancer cell lines. **(a)** Schematic illustration of the drug treatment experiment. Samples were processed as part of the same workflow shown in Fig. 1. Images created using Illustrator. **(b)** Correlations of RPPA data derived from antibodies recognising the same antigen class (like antigens) were compared to those derived from all antibodies used in the integrated multi-platform RPPA dataset. **(c)** For like antigens, correlations of RPPA data derived from the same antibodies were compared to those derived from different antibodies. **(d,e)** Correlations between RPPA data generated at the different RPPA platforms were compared for data from the same antibodies **(d)** and different antibodies recognising like antigens **(e)**. **(f)** Correlations of RPPA data derived from different antibodies recognising like antigens generated on the same RPPA platform were compared to those generated on different RPPA platforms. For **(b–f)**, kernel density estimates of Spearman rank correlation coefficients for every pair-wise combination of unique antibody identifiers were computed. Spearman rank correlation coefficient data points for each set of comparisons are indicated by rug plots. For each set of comparisons, the median Spearman rank correlation coefficient (r_s) is shown (dashed lines). *NS* not significant. For further details, see Supplementary Fig. S3.

that of phosphorylated Her2 and EGFR and downstream signalling molecules Akt and Erk1/2 (Fig. 4a,b, Supplementary Fig. S4). In contrast, dimensionality-reduced RPPA data for MCF7 cells, which do not overexpress Her2 or EGFR, did not display a large shift in feature space away from control conditions, in keeping with the lack of response to lapatinib treatment of MCF7 cells (Supplementary Fig. S4). For cells treated with selumetinib, a strong reduction in phosphorylated Erk1/2—which is activated upon phosphorylation by MEK⁴⁷—was observed in MEK inhibitor-sensitive MDA-MB-231 cells analysed at all RPPA platforms (Fig. 4a,b), whereas SKBR3 cells, which are not as sensitive to selumetinib, displayed a minimal shift in feature space for selumetinib-treated samples (Fig. 4a). In some cell lines, upregulation of phosphorylated MEK1/2 was observed upon selumetinib treatment, particularly after treatment for 24 h, representing the likely effects of reduced negative feedback on

the upstream MAPK pathway as a result of transiently inhibited Erk1/2 upon MEK inhibition^{48,49}. In general, for drug-sensitive cell lines, shifts in feature space were more pronounced for cells treated for 24 h as compared to 20 min, implying that the modulation of signalling pathways was enhanced when cells were challenged with drugs for longer, enabling modelling of the dynamic signalling landscape (Supplementary Fig. S4). Furthermore, in drug-resistant cell lines, we observed the emergence of potential resistance mechanisms, such as the activation of phosphorylated EGFR, Her2 and Akt in SKBR3 cells treated with selumetinib (Supplementary Fig. S4). These analyses show that the RPPA data represent expected changes in breast cancer cell responses to the pharmacological inhibitors tested, capturing relevant signalling dynamics, and serve as a suitable platform for the integrative multi-platform RPPA analysis of drug-treated cells.

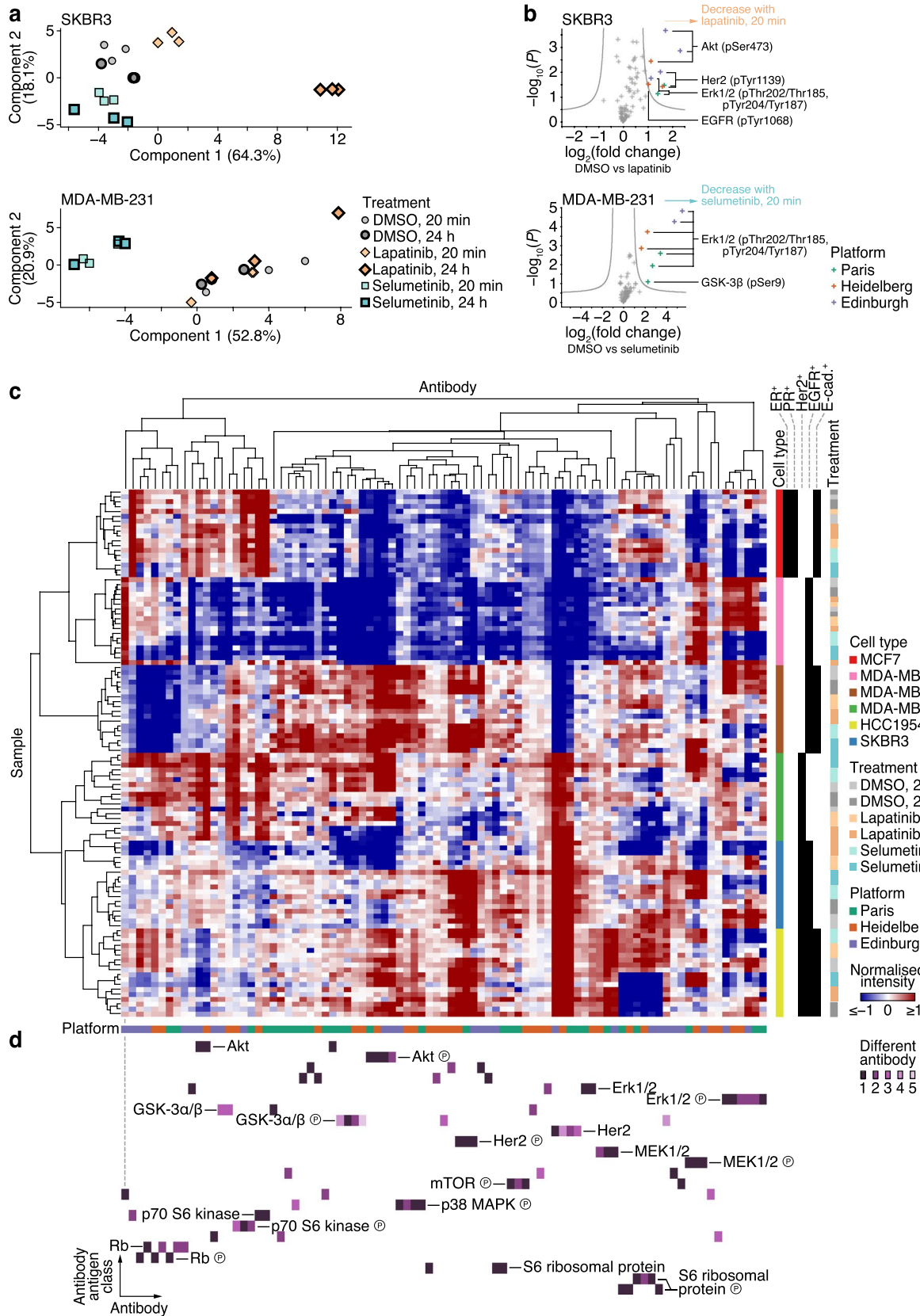
We next analysed the integrated RPPA dataset of drug-treated cell lines using unsupervised cluster analysis. Two-dimensional hierarchical clustering partitioned samples by breast cancer cell line, which were further partitioned by treatment condition (for respective drug-sensitive cells), with replicate samples clustering together, indicating robust data-driven grouping of the dataset (Fig. 4c, Supplementary Fig. S5, Supplementary Table S6). Clustered antibody antigen mapping, driven by this unsupervised dataset partitioning, identified clusters of antibodies targeting the same antigen (Fig. 4d, Supplementary Fig. S5). As for the analysis of the cells cultured under control conditions (Fig. 2, Supplementary Fig. S2), expression of many of the antigens tested (75%) clustered with expression of the same antigen determined by at least one other RPPA platform (Fig. 4d). Furthermore, the expression of several of the antigens for which distinct antibodies were used (56%) clustered with the same antigen detected by a different antibody (Fig. 4d). Together, these results indicate that integrative RPPA analysis of drug-treated cells can identify concordant profiles of response to pharmacological inhibition using distinct antibodies and different RPPA platforms. This suggests that the robustness of RPPA technology is suitable for the characterisation of pathway signalling networks across international laboratories.

Discussion

With RPPA technology poised for adoption into routine clinical laboratory assays, there is a need to assess reproducibility and variation between RPPA data derived from different platforms. Herein, we employed a collaborative RPPA-based proteomics approach to evaluate the consistency of results obtained from the same samples using different RPPA workflows. We combined the RPPA data derived from multiple research sites to assess inter-platform variation and found that different RPPA platforms using distinct set-ups yield remarkably consistent results, including when several different antibodies are used to recognise the same antigen (protein or phosphoprotein) of interest. Indeed, antigens detected by different antibodies used at different RPPA platforms were, in general, almost as well correlated as those used at the same RPPA platform. These observations strongly suggest that the different instrumental set-ups and analytical workflows used at these representative RPPA platforms do not preclude the generation of comparable and reproducible data when using high-quality, validated antibodies.

Using different workflows, the layout of samples spotted on arrays differed among the three RPPA platforms, which prevented application of the same automated data normalisation method. Each research site therefore applied their own in-house data normalisation procedure tailored for the respective RPPA platform. All platforms normalised signal intensities for total amounts of printed protein, but the way they accounted for sample dilutions differed. The Paris platform applied non-parametric curve fitting to the serial dilutions of each sample, the Heidelberg platform fitted curves for control samples only and reported experimental samples to these curves and the Edinburgh platform computed a linear fit of the serially diluted samples. Despite these different approaches, we show that normalised data improves the distinction between concordant data (derived from antibodies recognising the same antigen class) and non-concordant data (derived from all antibodies regardless of target), as compared to raw data. Future efforts to develop normalisation pipelines that are compatible with multiple array layouts may further improve data reproducibility among platforms and expand opportunities for cross-platform validation of RPPA technology. Such cross-platform validation may have utility in the appraisal of robust markers of disease and therapeutic response and their application as prognostic or predictive biomarkers.

There is an outstanding need for the development of robust markers of response and resistance to targeted cancer therapy⁵⁻⁷. Proteomic and phosphoproteomic datasets are well placed to complement genetics-based biomarker strategies by providing additional information on activation states of dynamic pathway signalling. However, the application of proteomic technologies presents a number of challenges, including consistent high-quality sample preparation, sensitive detection of low-abundance proteins and post-translational modifications, high sample throughput at reasonable cost and rapid turnaround time necessary for clinical application or drug discovery and development pipelines. The development of RPPA workflows attempts to address many of these challenges, yet the reproducibility of RPPA data generation and analysis across distinct RPPA platforms and research centres has not been extensively evaluated. We used an integrative RPPA approach to characterise a range of human breast cancer cell lines and their biochemical responses to two clinically relevant cancer drugs. The cell lines were chosen to represent different molecular subtypes of breast cancer, each of which having a different prognosis and treatment response⁵⁰. The sensitivity of these cell lines towards lapatinib and selumetinib and the expected changes in major signalling pathways are known⁵¹⁻⁵³ and thus served as benchmarks in this study. We demonstrated that RPPA technology can identify expected protein markers for response to treatment and resistance in a robust and platform-independent manner. Although we analysed cell lines herein to enable benchmarking, RPPA is routinely applied to clinical samples, including small biopsies, on the platforms used in this study. In such cases, the amount of lysis buffer is adapted to the amount and the cellularity of the tissue in order to obtain sufficiently concentrated samples. We therefore expect that RPPA can robustly assess response to treatment and resistance independently of the analysed samples. Understanding how resistance can be predicted and prevented is a major therapeutic challenge, and the use of proteomic approaches such as RPPA will, by



◀ **Figure 4.** Integrative multi-platform RPPA analysis of drug-treated breast cancer cell lines. (a) Principal component analyses of integrated RPPA data of SKBR3 cells (top) or MDA-MB-231 cells (bottom) treated with lapatinib, selumetinib or vehicle control (DMSO) at two timepoints. (b) Volcano plots of RPPA data of SKBR3 cells treated with lapatinib (top) or MDA-MB-231 cells treated with selumetinib (bottom) compared to those treated with vehicle control (DMSO) for 20 min. Differentially regulated phosphoproteins are labelled. Grey curves indicate 5% false discovery rate ($n = 3$ independent samples). (c) Integrated multi-platform RPPA data of drug-treated breast cancer cell lines were clustered on the basis of antibody-wise and sample-wise dissimilarities (Spearman rank correlation coefficient-based distance). Annotation bars indicate cell type, cell type receptor status, drug treatment and RPPA platform. (d) Clustered antibody antigen map for all antibodies used in the integrative analysis. The map is aligned with the hierarchical clustering results in c [grey dashed line above the left-most antibody indicates alignment of the first antibody (column) end-node] and coloured and ordered as for Fig. 2. For further details, see Supplementary Figs. S4 and S5 and Supplementary Table S6.

defining the functional state of cells and tissues, enable the validation and assessment of resistance mechanisms in clinical samples^{5,54}.

High attrition rates in clinical drug development present significant challenges to drug developers, with only one in eight oncology drugs that enter clinical development in phase I achieving US Food and Drug Administration approval, and a 1-in-15 success rate when these candidate drugs are under evaluation in secondary oncology indications⁵⁵. The development of robust biomarkers is thus becoming an essential component of new clinical trial designs to guide patient selection, optimise dosing schedules and minimise ineffective or over-treatment. For many complex diseases, biomarkers at the genetic, proteomic, metabolomic and phenotypic levels are required to characterise individual patient disease and response to therapy sufficiently. Integration of multiple biomarker modalities with emerging computational and statistical approaches represents the future direction of personalised medicine strategies. However, the successful implementation of personalised medicine is dependent upon the validation and reproducibility of biomarker tests performed across distinct research centres and national boundaries.

Our data show that RPPA analyses of drug-treated breast cancer cells using distinct antibodies and different RPPA platforms can identify robust profiles of protein markers reporting signalling pathway responses to pharmacological inhibition. This suggests that the consistency of RPPA-based assays will enable the validation and assessment of treatment response and resistance mechanisms in clinical samples across international laboratories. These data provide, to our knowledge, the first extensive cross-platform validation of RPPA technology, which paves the way for further investigation and improvement of technology robustness.

Methods

Cell lines and cell lysis. MCF7, MDA-MB-231, MDA-MB-468, MDA-MB-453, HCC1954 and SKBR3 breast cancer cells were purchased from American Type Culture Collection and grown according to supplied instructions (Supplementary Table S1). For the preparation of cell lysates, cells were washed twice with ice-cold phosphate-buffered saline (PBS). Laemmli buffer [50 mM Tris-HCl (pH 6.8), 2% sodium dodecyl sulfate, 5% glycerol, 2 mM DTT, 2.5 mM EDTA, 2.5 mM EGTA, supplemented with 4 mM sodium orthovanadate, 20 mM sodium fluoride, Halt phosphatase inhibitor cocktail (Perbio) and cOmplete protease inhibitor cocktail (Roche)] was incubated at 100 °C for 5 min and applied directly to cells. Samples were immediately incubated at 100 °C for 10 min. Lysates were passed through a 25-gauge needle five times and clarified by centrifugation (18,000×g, 10 min, room temperature). Clarified lysates were aliquoted and snap-frozen in liquid nitrogen prior to shipment to the various research sites. Protein concentration was determined using a reducing agent-compatible BCA kit (Pierce).

Pharmacological inhibitor treatment. Lapatinib and selumetinib (Selleck Chemicals) were prepared as 10 mM stock solutions in DMSO. Cells were treated with 1 μM lapatinib, 1 μM selumetinib or DMSO in growth medium for 20 min or 24 h. Control cells were treated with DMSO in growth medium for 20 min.

RPPA analysis. Samples were analysed at each research site using the respective in-house RPPA platforms as summarised in Supplementary Table S2. For the Paris and Edinburgh platforms, all biological triplicate lysates were serially diluted to produce a dilution series comprising four serial twofold dilutions of each sample. For the Heidelberg platform, biological triplicate DMSO-treated control lysates were serially diluted to produce a control dilution series comprising six serial twofold dilutions of each control sample to enable representative dilution series intercept correction using RPPAnalyzer as described previously⁵⁶. We confirmed that >99% of data points derived from undiluted samples at the Heidelberg platform were within the dynamic range of the representative dilution series (Supplementary Fig. S5). Samples were spotted onto Grace Bio-Labs ONCYTE nitrocellulose-coated slides (Sigma-Aldrich) in technical duplicate or triplicate under conditions of constant 70% humidity using an Aushon 2470 arrayer (Aushon Biosystems). Slides were hydrated in deionised water and blocked with blocking buffer (Supplementary Table S2). Slides were washed with Tris-buffered saline containing 0.1% Tween 20 (TBS-T) and incubated with validated primary antibodies diluted in blocking buffer at room temperature for 1 h or at 4 °C overnight (Supplementary Table S3). Slides were washed with TBS-T and probed with secondary antibodies diluted in blocking buffer at room temperature for 30 min or 1 h. To amplify the signal, if applicable, slides were incubated with biotin and peroxidase blocking reagents (Dako) prior to primary antibody incubation and then with Bio-Rad Amplification Reagent (Bio-Rad) at room temperature for 15 min after secondary antibody incubation (Supplementary Table S2). Slides were washed with TBS-T. For staining

of total protein with SYPRO Ruby, slides were washed once with 7% acetic acid, 10% methanol (15 min), twice with deionised water, once with SYPRO Ruby (Thermo Fisher Scientific) and five times with deionised water. For staining of total protein with Fast Green FCF, slides were washed once with deionised water, once with 1% sodium hydroxide (15 min), twice with deionised water, once with 7% acetic acid, 30% methanol (15 min), once with 0.0025% Fast Green FCF (Sigma-Aldrich), 7% acetic acid, 30% methanol (3 min), once with deionised water, once with 7% acetic acid, 30% methanol (15 min) and once with deionised water. Slides were allowed to dry at room temperature for 10 min prior to slide scanning. Slides were read using a GenePix 4000B (Molecular Devices), Odyssey (LI-COR Biosciences) or InnoScan 710-IR (Innopsys) scanner (Supplementary Table S2). The relative fluorescence intensity of each sample spot was quantified using MicroVigene (VigeneTech), GenePix Pro (Molecular Devices) or Mapix (Innopsys) software (Supplementary Table S2). For all platforms, signal intensities of < 1% of undiluted samples were below the lower limits of detection for all antibody antigens. Processed signal intensities were normalised using NormaCurve¹⁶, RPPAnalyzer^{33,56} or spot-by-spot division of antibody signal intensity by total protein stain signal intensity (Supplementary Table S2).

Dataset integration. We used RPPA data derived from all three RPPA platforms that had been normalised using the respective in-house normalisation procedure of each platform (Supplementary Table S2). Normalised RPPA data derived from each platform were binary-logarithm transformed, unless they were so transformed as part of the platform-specific normalisation procedure, and stored as matrices of transformed normalised data points (elements) arranged in rows of different samples and columns of different antibodies. For data derived from each platform, for each column of the matrix representing data for an antibody, the median of all samples was calculated and this was subtracted from each element in that column. Matrices of antibody-wise median-centred data derived from each platform were horizontally concatenated into a single matrix. Unique antibody identifiers were assigned to each distinct antibody based on antibody reference, and antibody antigens were classified to account for recognition of up to two related protein or phosphoprotein isoforms or family members (e.g. antibodies targeting Erk1 and Erk1/2 were classified as recognising Erk1/2) (Supplementary Table S3). Data for antibodies targeting the same antigen class used on all three RPPA platforms were used for dataset integration; antigen classes represented by data derived from fewer than three RPPA platforms were excluded from further analysis.

Unsupervised learning. Binary, agglomerative hierarchical cluster analyses of centred normalised abundances for proteins and phosphoproteins were performed using Cluster 3.0 (C Clustering Library, version 1.54)⁵⁷. Spearman rank correlation coefficients, Euclidean distances and Kendall tau coefficients were calculated and adapted as distances, if necessary. Distance matrices were built using pairwise average linkage. Hierarchical clustering results were visualised using Java TreeView (version 1.1.5r2)⁵⁸ and compiled using Illustrator (Adobe). Principal component analyses were performed using Python (version 3.7.4) or Perseus (version 1.5.2.6)⁵⁹.

Clustered antibody antigen mapping. For data-driven representation of antibody similarity across multiple RPPA platforms, we devised the clustered antibody antigen map. For all antibodies used in the integrative analysis, centred normalised abundances for proteins and phosphoproteins were clustered on the basis of Spearman rank correlation coefficient-based distance, Euclidean distance or Kendall tau coefficient-based distance using Cluster 3.0, computing distances with an average-linkage matrix. Clustered antibody (column) node memberships were stored for antibody mapping, and clustered antibodies were expanded in a second dimension according to antibody antigen classification. Antibodies targeting the same antigen class were indexed according to unique antibody identifier, enumerating from 1. A matrix of integer-indexed antibody identifier elements was generated according to clustered antibodies (columns) and corresponding antibody antigen classes (rows) (Supplementary Table S3). In this matrix, antibody (column) node memberships determined by clustering of RPPA data were preserved, and antibody antigen classes (rows) were ordered alphabetically. The resulting clustered antibody-antigen feature space was used to annotate the integrated multi-platform RPPA data. Mapping results were visualised using Java TreeView and compiled using Illustrator.

Statistical analyses. No statistical methods were used to pre-determine sample size. Spearman rank correlation coefficients were calculated for every pair-wise combination of antibody identifiers. Kernel density estimates were computed using R (version 3.4.1)⁶⁰. Median Spearman rank correlation coefficients were compared using Fisher transformation and two-sided *z*-tests. Differentially regulated proteins and phosphoproteins were compared using two-tailed Student's *t*-tests with artificial within-groups variance set to 1 and a permutation-based false discovery rate threshold of 5% (1,000 randomisations using Perseus).

Data availability

The datasets analysed during the current study are included in this published article (and its Supplementary Information files) or are available from the corresponding authors on reasonable request.

Received: 18 September 2019; Accepted: 11 March 2020

Published online: 15 December 2020

References

1. Aronson, S. J. & Rehm, H. L. Building the foundation for genomics in precision medicine. *Nature* **526**, 336–342 (2015).
2. Friedman, A. A., Letai, A., Fisher, D. E. & Flaherty, K. T. Precision medicine for cancer with next-generation functional diagnostics. *Nat. Rev. Cancer* **15**, 747–756 (2015).

3. Cancer Genome Atlas Network. Comprehensive molecular portraits of human breast tumours. *Nature* **490**, 61–70 (2012).
4. Wulfkühle, J. D. *et al.* Molecular analysis of HER2 signaling in human breast cancer by functional protein pathway activation mapping. *Clin. Cancer Res.* **18**, 6426–6435 (2012).
5. Mueller, C., Haymond, A., Davis, J. B., Williams, A. & Espina, V. Protein biomarkers for subtyping breast cancer and implications for future research. *Expert Rev. Proteomics* **15**, 131–152 (2018).
6. Giudice, G. & Petsalaki, E. Proteomics and phosphoproteomics in precision medicine: applications and challenges. *Brief. Bioinform.* **20**, 767–777 (2019).
7. Pierobon, M., Wulfkühle, J., Liotta, L. A. & Petricoin, E. F. III. Utilization of proteomic technologies for precision oncology applications. *Cancer Treat. Res.* **178**, 171–187 (2019).
8. Paweletz, C. P. *et al.* Reverse phase protein microarrays which capture disease progression show activation of pro-survival pathways at the cancer invasion front. *Oncogene* **20**, 1981–1989 (2001).
9. Akbani, R. *et al.* Realizing the promise of reverse phase protein arrays for clinical, translational, and basic research: a workshop report: the RPPA (Reverse Phase Protein Array) society. *Mol. Cell. Proteomics* **13**, 1625–1643 (2014).
10. Macleod, K. G., Serrels, B. & Carragher, N. O. Reverse phase protein arrays and drug discovery. *Methods Mol. Biol.* **1647**, 153–169 (2017).
11. Hsieh, H. J. *et al.* Systems biology approach reveals a link between mTORC1 and G2/M DNA damage checkpoint recovery. *Nat. Commun.* **9**, 3982 (2018).
12. Ramaswamy, A. *et al.* Application of protein lysate microarrays to molecular marker verification and quantification. *Proteome Sci.* **3**, 9 (2005).
13. Tibes, R. *et al.* Reverse phase protein array: validation of a novel proteomic technology and utility for analysis of primary leukemia specimens and hematopoietic stem cells. *Mol. Cancer Ther.* **5**, 2512–2521 (2006).
14. Grote, T. *et al.* Validation of reverse phase protein array for practical screening of potential biomarkers in serum and plasma: accurate detection of CA19-9 levels in pancreatic cancer. *Proteomics* **8**, 3051–3060 (2008).
15. Dupuy, L. *et al.* A highly sensitive near-infrared fluorescent detection method to analyze signalling pathways by reverse-phase protein array. *Proteomics* **9**, 5446–5454 (2009).
16. Troncale, S. *et al.* NormaCurve: a SuperCurve-based method that simultaneously quantifies and normalizes reverse phase protein array data. *PLoS ONE* **7**, e38686 (2012).
17. Grubb, R. L. *et al.* Pathway biomarker profiling of localized and metastatic human prostate cancer reveal metastatic and prognostic signatures. *J. Proteome Res.* **8**, 3044–3054 (2009).
18. Gonzalez-Angulo, A. M. *et al.* Functional proteomics can define prognosis and predict pathologic complete response in patients with breast cancer. *Clin. Proteomics* **8**, 11 (2011).
19. Murakoshi, Y. *et al.* Plasma biomarker discovery and validation for colorectal cancer by quantitative shotgun mass spectrometry and protein microarray. *Cancer Sci.* **102**, 630–638 (2011).
20. Hayashi, N. *et al.* Reverse-phase protein array for prediction of patients at low risk of developing bone metastasis from breast cancer. *Oncologist* **19**, 909–914 (2014).
21. Bernhardt, S. *et al.* Proteomic profiling of breast cancer metabolism identifies SHMT2 and ASCT2 as prognostic factors. *Breast Cancer Res.* **19**, 112 (2017).
22. Hutter, G. *et al.* Reverse phase protein arrays enable glioblastoma molecular subtyping. *J. Neurooncol.* **131**, 437–448 (2017).
23. Lièvre, A. *et al.* Protein biomarkers predictive for response to anti-EGFR treatment in RAS wild-type metastatic colorectal carcinoma. *Br. J. Cancer* **117**, 1819–1827 (2017).
24. Aslan, O. *et al.* Preclinical evaluation and reverse phase protein array-based profiling of PI3K and MEK inhibitors in endometrial carcinoma in vitro. *BMC Cancer* **18**, 168 (2018).
25. Faham, N., Zhao, L. & Welm, A. L. mTORC1 is a key mediator of RON-dependent breast cancer metastasis with therapeutic potential. *NPJ Breast Cancer* **4**, 36 (2018).
26. Teo, K. *et al.* E-cadherin loss induces targetable autocrine activation of growth factor signalling in lobular breast cancer. *Sci. Rep.* **8**, 15454 (2018).
27. Byron, A. Reproducibility and crossplatform validation of reverse-phase protein array data. *Adv. Exp. Med. Biol.* **1188**, 181–201 (2019).
28. Mircean, C. *et al.* Robust estimation of protein expression ratios with lysate microarray technology. *Bioinformatics* **21**, 1935–1942 (2005).
29. Hu, J. *et al.* Non-parametric quantification of protein lysate arrays. *Bioinformatics* **23**, 1986–1994 (2007).
30. Anderson, T., Wulfkühle, J., Liotta, L., Winslow, R. L. & Petricoin, E. 3rd. Improved reproducibility of reverse-phase protein microarrays using array microenvironment normalization. *Proteomics* **9**, 5562–5566 (2009).
31. Neeley, E. S., Kornblau, S. M., Coombes, K. R. & Baggerly, K. A. Variable slope normalization of reverse phase protein arrays. *Bioinformatics* **25**, 1384–1389 (2009).
32. Zhang, L. *et al.* Serial dilution curve: a new method for analysis of reverse phase protein array data. *Bioinformatics* **25**, 650–654 (2009).
33. Mannsperger, H. A., Gade, S., Henjes, F., Beissbarth, T. & Korf, U. RPPAnalyzer: analysis of reverse-phase protein array data. *Bioinformatics* **26**, 2202–2203 (2010).
34. Li, B., Liang, F., Hu, J. & He, A. X. Reno: regularized non-parametric analysis of protein lysate array data. *Bioinformatics* **28**, 1223–1229 (2012).
35. Neeley, E. S., Baggerly, K. A. & Kornblau, S. M. Surface adjustment of reverse phase protein arrays using positive control spots. *Cancer Inform.* **11**, 77–86 (2012).
36. Kaushik, P. *et al.* Spatial normalization of reverse phase protein array data. *PLoS ONE* **9**, e97213 (2014).
37. List, M. *et al.* Microarray R-based analysis of complex lysate experiments with MIRACLE. *Bioinformatics* **30**, i631–i638 (2014).
38. Liu, W., Ju, Z., Lu, Y., Mills, G. B. & Akbani, R. A comprehensive comparison of normalization methods for loading control and variance stabilization of reverse-phase protein array data. *Cancer Inform.* **13**, 109–117 (2014).
39. Ju, Z. *et al.* Development of a robust classifier for quality control of reverse-phase protein arrays. *Bioinformatics* **31**, 912–918 (2015).
40. Sun, M., Lai, D., Zhang, L. & Huang, X. Modified SuperCurve method for analysis of reverse-phase protein array data. *J. Comput. Biol.* **22**, 765–769 (2015).
41. Gallagher, R. I. & Espina, V. Reverse phase protein arrays: mapping the path towards personalized medicine. *Mol. Diagn. Ther.* **18**, 619–630 (2014).
42. Masuda, M. & Yamada, T. Signaling pathway profiling by reverse-phase protein array for personalized cancer medicine. *Biochim. Biophys. Acta* **1854**, 651–657 (2015).
43. Spector, N. L. *et al.* Study of the biologic effects of lapatinib, a reversible inhibitor of ErbB1 and ErbB2 tyrosine kinases, on tumor growth and survival pathways in patients with advanced malignancies. *J. Clin. Oncol.* **23**, 2502–2512 (2005).
44. Yeh, T. C. *et al.* Biological characterization of ARRY-142886 (AZD6244), a potent, highly selective mitogen-activated protein kinase kinase 1/2 inhibitor. *Clin. Cancer Res.* **13**, 1576–1583 (2007).
45. Hegde, P. S. *et al.* Delineation of molecular mechanisms of sensitivity to lapatinib in breast cancer cell lines using global gene expression profiles. *Mol. Cancer Ther.* **6**, 1629–1640 (2007).

46. Imami, K. *et al.* Temporal profiling of lapatinib-suppressed phosphorylation signals in EGFR/HER2 pathways. *Mol. Cell. Proteomics* **11**, 1741–1757 (2012).
47. Dhillon, A. S., Hagan, S., Rath, O. & Kolch, W. MAP kinase signalling pathways in cancer. *Oncogene* **26**, 3279–3290 (2007).
48. Pratilas, C. A. *et al.* (V600E)BRAF is associated with disabled feedback inhibition of RAF-MEK signaling and elevated transcriptional output of the pathway. *Proc. Natl. Acad. Sci. USA* **106**, 4519–4524 (2009).
49. Lito, P. *et al.* Disruption of CRAF-mediated MEK activation is required for effective MEK inhibition in KRAS mutant tumors. *Cancer Cell* **25**, 697–710 (2014).
50. Sørlie, T. *et al.* Gene expression patterns of breast carcinomas distinguish tumor subclasses with clinical implications. *Proc. Natl. Acad. Sci. USA* **98**, 10869–10874 (2001).
51. Konecny, G. E. *et al.* Activity of the dual kinase inhibitor lapatinib (GW572016) against HER-2-overexpressing and trastuzumab-treated breast cancer cells. *Cancer Res.* **66**, 1630–1639 (2006).
52. Garon, E. B. *et al.* Identification of common predictive markers of in vitro response to the Mek inhibitor selumetinib (AZD6244; ARRY-142886) in human breast cancer and non-small cell lung cancer cell lines. *Mol. Cancer Ther.* **9**, 1985–1994 (2010).
53. O'Neill, F. *et al.* Gene expression changes as markers of early lapatinib response in a panel of breast cancer cell lines. *Mol. Cancer* **11**, 41 (2012).
54. Creedon, H. *et al.* Exploring mechanisms of acquired resistance to HER2 (human epidermal growth factor receptor 2)-targeted therapies in breast cancer. *Biochem. Soc. Trans.* **42**, 822–830 (2014).
55. Hay, M., Thomas, D. W., Craighead, J. L., Economides, C. & Rosenthal, J. Clinical development success rates for investigational drugs. *Nat. Biotechnol.* **32**, 40–51 (2014).
56. von der Heyde, S. *et al.* RPPanalyzer toolbox: an improved R package for analysis of reverse phase protein array data. *Biotechniques* **57**, 125–135 (2014).
57. de Hoon, M. J. L., Imoto, S., Nolan, J. & Miyano, S. Open source clustering software. *Bioinformatics* **20**, 1453–1454 (2004).
58. Saldanha, A. J. Java Treeview—extensible visualization of microarray data. *Bioinformatics* **20**, 3246–3248 (2004).
59. Tyanova, S. *et al.* The Perseus computational platform for comprehensive analysis of (prote)omics data. *Nat. Methods* **13**, 731–740 (2016).
60. R Core Team. *R: A Language and Environment for Statistical Computing.* (R Foundation for Statistical Computing, 2017).

Acknowledgements

We thank Philippe Hupé for helpful scientific input, Patrick Poulet and Stéphane Liva for development and maintenance of data management tools at Institut Curie and Andrew H. Sims for discussions. A.B. was supported by Cancer Research UK. K.G.M. is supported by the Cancer Research UK Edinburgh Centre award (C157/A25140). The Institut Curie RPPA platform is supported by Cancéropôle Ile-de-France.

Author contributions

A.B., N.O.C., U.K., B.S. and L.d.K. conceived the study and designed the experiments. S.B., B.O., A.C. and K.G.M. generated the data. A.B., S.B., K.G.M., V.S., B.S. and L.d.K. analysed and interpreted the data. A.B. designed and implemented data integration and prepared the figures. A.B., N.O.C. and L.d.K. wrote the manuscript. All authors critically reviewed and approved the manuscript.

Competing interests

The authors declare no competing interests.

Additional information

Supplementary information is available for this paper at <https://doi.org/10.1038/s41598-020-77335-0>.

Correspondence and requests for materials should be addressed to A.B. or L.d.K.

Reprints and permissions information is available at www.nature.com/reprints.

Publisher's note Springer Nature remains neutral with regard to jurisdictional claims in published maps and institutional affiliations.



Open Access This article is licensed under a Creative Commons Attribution 4.0 International License, which permits use, sharing, adaptation, distribution and reproduction in any medium or format, as long as you give appropriate credit to the original author(s) and the source, provide a link to the Creative Commons licence, and indicate if changes were made. The images or other third party material in this article are included in the article's Creative Commons licence, unless indicated otherwise in a credit line to the material. If material is not included in the article's Creative Commons licence and your intended use is not permitted by statutory regulation or exceeds the permitted use, you will need to obtain permission directly from the copyright holder. To view a copy of this licence, visit <http://creativecommons.org/licenses/by/4.0/>.

© The Author(s) 2020